9th ANKARA INTERNATIONAL AEROSPACE CONFERENCE **AIAC-2017-047**
20-22 September 2017 - METU, Ankara TURKEY

# LARGE EDDY SIMULATION OF WALL-BOUNDED TURBULENT FLOWS

Dogukan T. Karahan[*], Sarp Er[†] and Ayse G. Gungor[‡]
Faculty of Aeronautics and Astronautics, Istanbul Technical University, Istanbul, Turkey

## ABSTRACT

*The aim of this study is to introduce a new in-house, parallel, compressible large eddy simulation solver lestr3d, to be used for wall-bounded turbulent problems encountered in the aerospace field. Parallelization of the solver shows a good scaling performance up to 512 cores on different platforms. The solver is benchmarked by simulating lid-driven cavity flow and the results are compared against available direct numerical simulation and experimental data. Moreover, the capabilities of the solver is further investigated via flow over a T106 turbine blade. Instantaneous results about the nature of the flow and mean pressure coefficient are presented. Current results show promising capabilities of the solver in wall-bounded complex turbulent flows.*

## INTRODUCTION

Aerospace industry has now shifted to investigation of spatial and temporal dynamics of turbulence instead of relying on steady state solutions to the governing equations of fluid dynamics due to increased design demands. Thanks to development of massively parallel computational platforms, it is now possible to perform detailed investigation of complex flow problems by means of computational methods. However, direct simulation of real life problems is still exceeding the capabilities of current technology [Lacaze and Oefelein, 2015]. On the other hand, large eddy simulation (LES) has become a promising technique to study spacetime history of turbulence dynamics it has been widely employed in the aerospace field [Andersson et al, 2015; Falese et al, 2014; Gourdain et al, 2009b]. Current trend in aerospace community is to depend on in-house codes [Url-3, 2017; Url-4, 2017; Url-5, 2017] in both academic and industrial applications. Therefore, the aim of this work is to introduce a new in-house LES solver that is capable of solving wall-bounded turbulent flow problems encountered in the aerospace industry.

Firstly, the governing equations for compressible LES are presented along with the sub-grid scale models required to close the LES equations. Details of the new solver are given by explaining the numerical methods used. Then the scalability performance of the code is shown. The capabilities of the solver are presented by using the results obtained from LES of lid-driven cavity and flow over T106 blade. Finally concluding remarks are made in the last section.

[*]MSc. Student in Aero. and Astro. Eng., Email: karahand@itu.edu.tr
[†]MSc. Student in Aero. and Astro. Eng, Email: ersa@itu.edu.tr
[‡]Assist. Prof, Email: ayse.gungor@itu.edu.tr

## GOVERNING EQUATIONS

Compressible LES equations are obtained through application of a spatial filter to the Navier-Stokes (NS) equations. Filtering procedure on any flow variable, $\Psi$, results in sum of a large-scale (resolvable) component, $\overline{\Phi}$, and a small scale (sub-grid) component, $\Phi'$; i.e. $\Phi = \overline{\Phi} + \Phi'$. The separation between large and small scales are determined by the filter width size $\overline{\Delta}$. In this study, box filter is employed and the the filter is assumed to commute with differentiation.

In compressible flows, velocity and energy field are represented by density averaged sense to avoid extra sub-grid terms in the governing equations. A Favre-filtered quantity $\tilde{\Psi}$ in the flow field is represented as $\tilde{\Psi} = \overline{\rho\Psi}/\overline{\rho}$ where $\rho$ represents density of the fluid. Using above information, continuity, momentum, and total energy equations can be written (respectively) as;

$$\frac{\partial \overline{\rho}}{\partial t} + \frac{\partial \overline{\rho}\tilde{u}_i}{\partial x_i} = 0; \tag{1}$$

$$\frac{\partial \overline{\rho}\tilde{u}_i}{\partial t} + \frac{\partial}{\partial x_j}[\overline{\rho}\tilde{u}_i\tilde{u}_j + \overline{p}\delta_{ij} - \tilde{\tau}_{ij} + \tau_{ij}^{sgs}] = 0; \tag{2}$$

$$\frac{\partial \overline{\rho}\tilde{E}}{\partial t} + \frac{\partial}{\partial x_i}[(\overline{\rho}\tilde{E} + \overline{p})\tilde{u}_i + \tilde{q}_i - \tilde{u}_j\tilde{\tau}_{ij} + H_i^{sgs}] = 0. \tag{3}$$

Here, $i$ and $j$ are indices having values of $1, 2, 3$ which are used in accordance with Einstein's summation convention. Time, spatial coordinates, velocity, pressure, viscous stress tensor, sub-grid scale(sgs) stress tensor, energy, heat flux, and sgs heat flux are represented by $t$, $x_i$ (or $x_j$), $\tilde{u}_i$ (or $\tilde{u}_j$), $\overline{p}$, $\tilde{\tau}_{ij}$, $\tau_{ij}^{sgs}$, $\tilde{E}$, $\tilde{q}_i$, and $H_i^{sgs}$, respectively. Fluid is assumed to behave as a calorically perfect gas and as a Newtonian fluid.

The effect of sub-grid scale dynamics appear as the sgs stress tensor, $\tau_{ij}^{sgs}$ and sgs heat flux $H_i^{sgs}$ in the LES equations and has to be modelled. Compressible extension [Erlebacher et al, 1992] of Smagorinsky model [Smagorinsky, 1963] is used as an sgs tensor model;

$$\tau_{ij}^{sgs} = -\mu_t\Big(2\tilde{S}_{ij} - \frac{2}{3}\tilde{S}_{mm}\delta_{ij}\Big) + \frac{2}{3}\overline{\rho}k^{sgs}\delta_{ij} \tag{4}$$

Terms in this equation can be expressed as; $\mu_t$ sub-grid scale viscosity, $\tilde{S}_{mm}$ resolved strain rate tensor and $k^{sgs}$ sub-grid scale kinetic energy. Relations for these terms are;

$$\mu_t = C_R\overline{\rho}\overline{\Delta}^2\sqrt{\tilde{S}_{mn}\tilde{S}_{mn}} \tag{5}$$

$$k^{sgs} = C_I\overline{\Delta}^2\tilde{S}_{mn}\tilde{S}_{mn} \tag{6}$$

where $C_R$ and $C_l$ are model coefficients and $\overline{\Delta}$ is the filter width defined as the cubic root of cell volume.

The unknown sgs enthalpy flux term in the energy equation is modelled with temperature gradient approach [Andersson et al, 2015];

$$H_i^{sgs} = -C_p\frac{\mu_t}{Pr_t}\frac{\partial\tilde{T}}{\partial x_i} \tag{7}$$

Here, $C_p$ is the specific heat and $Pr_t$ is sub-grid scale Prandtl number which is taken as unity in this study.

## NUMERICAL METHOD

The developed solver, named after *lestr3d*, is capable of solving non-reactive subsonic compressible gas flows in Cartesian coordinates. The parallel code is written in FORTRAN and it relies on Message-Passing Interface (MPI) libraries for multi-core applications. Domain decomposition is carried out using METIS [Karypis and Kumar, 1999] software.

The finite volume formulation of the compressible LES equations in integral form can be written as;

$$\frac{\partial}{\partial t}\int_{\Omega}\vec{Q}\mathrm{d}\Omega + \oint_{S}(\vec{F}_c - \vec{F}_v - \vec{F}^{sgs})\mathrm{d}S = 0. \tag{8}$$

Conservative flux vector $\vec{Q}$ which is being stored at the cell center for each element is;

$$\vec{Q} = \begin{bmatrix}\overline{\rho} & \overline{\rho}\tilde{u} & \overline{\rho}\tilde{v} & \overline{\rho}\tilde{w} & \overline{\rho}\tilde{E}\end{bmatrix}^T$$

Also convective, viscous and sgs flux vectors($\vec{F}_c$, $\vec{F}_v$, $\vec{F}^{sgs}$) can be written respectively as;

$$\vec{F}_c = \begin{bmatrix}\overline{\rho}V \\ \overline{\rho}\tilde{u}V + n_x\overline{p} \\ \overline{\rho}\tilde{v}V + n_y\overline{p} \\ \overline{\rho}\tilde{w}V + n_z\overline{p} \\ (\overline{\rho}\tilde{E} + \overline{p})V\end{bmatrix}, \qquad \vec{F}_v = \begin{bmatrix}0 \\ n_x\tilde{\tau}_{xx} + n_y\tilde{\tau}_{xy} + n_z\tilde{\tau}_{xz} \\ n_x\tilde{\tau}_{yx} + n_y\tilde{\tau}_{yy} + n_z\tilde{\tau}_{yz} \\ n_x\tilde{\tau}_{zx} + n_y\tilde{\tau}_{zy} + n_z\tilde{\tau}_{zz} \\ n_x\tilde{\Theta}_x + n_y\tilde{\Theta}_y + n_z\tilde{\Theta}_z\end{bmatrix},$$

$$\vec{F}^{sgs} = \begin{bmatrix}0 \\ n_x\tau_{xx}^{sgs^\circ} + n_y\tau_{xy}^{sgs^\circ} + n_z\tau_{xz}^{sgs^\circ} \\ n_x\tau_{yx}^{sgs^\circ} + n_y\tau_{yy}^{sgs^\circ} + n_z\tau_{yz}^{sgs^\circ} \\ n_x\tau_{zx}^{sgs^\circ} + n_y\tau_{zy}^{sgs^\circ} + n_z\tau_{zz}^{sgs^\circ} \\ n_xH_x^{sgs^\circ} + n_yH_y^{sgs^\circ} + n_zH_z^{sgs^\circ}\end{bmatrix}.$$

LES equations are discetized on unstructured grids. Second-order central scheme is employed for spatial discretization.

In order to prevent spurious oscillations due to central scheme, unstructured extension of Jameson-Schmidt-Turkel scheme(JST) [Frink, 1994] is implemented to the code as an artificial dissipation. The discrete form of equation (8) with the addition of artificial dissipation effect on the right-hand side is;

$$\frac{\partial\vec{Q}_i}{\partial t} = -\frac{1}{\Omega_i}\left(\sum_{J=1}^{N_F}\vec{F}_{c,J}S_J - \sum_{J=1}^{N_F}\vec{F}_{v,J}S_J - \sum_{J=1}^{N_F}\vec{F}_J^{sgs}S_J - \vec{D}_{JST,i}\right) \tag{9}$$

where, $N_f$ is the number of faces that defines each unstructured element and $J$ index is used to denote the calculated variables on faces. The artificial dissipation vector $\vec{D}_{JST,i}$ can be written as;

$$\vec{D}_{JST,i} = \sum_{J=1}^{N_F}(\hat{\Lambda}_c)_J\epsilon_J^{(2)}\theta_J(\vec{Q}_k - \vec{Q}_i) - \sum_{J=1}^{N_F}(\hat{\Lambda}_c)_J\epsilon_J^{(4)}\theta_J\big[L(\vec{Q}_k) - L(\vec{Q}_i)\big] \tag{10}$$

where, indices $i$ and $k$ stands for the elements on the left and right of the face, $(\hat{\Lambda}_c)_J$ is the convective spectral radius, $\epsilon_J^{(2)}$and $\epsilon_J^{(4)}$ are coefficients, $\theta_J$ is the geometrical constant and $L(\vec{Q}_k)$ and $L(\vec{Q}_i)$ are the pseudo-Laplacians of the conservative flux vectors evaluated at the cell centers. Coefficients; $\epsilon_J^{(2)}$and $\epsilon_J^{(4)}$ are determined by using the following relations;

$$\epsilon_J^{(2)} = k^{(2)}\max(\Upsilon_i, \Upsilon_k) \tag{11}$$

$$\epsilon_J^{(4)} = \max[0, (k^{(4)} - \epsilon_J^{(2)})] \tag{12}$$

In these relations, $\Upsilon_i$, $\Upsilon_k$ are pressure sensors at neighbouring elements and $k^{(2)}$, $k^{(4)}$ are JST dissipation constants.

Explicit time integration is carried out using five-stage Runge-Kutta scheme. Ghost cell methodology is carried out for the application of boundary conditions.

## SCALABILITY OF *lestr3d*

For better utilizing the computational resources that are in reach, solver is developed with the capability of conducting simulations using multiple cores. It enables to use grids with large number of elements and still be able to make the calculations in a reasonable time with the help of parallelization of the task. Scalability performance, which will be measured with speed-up in this section becomes important when a parallel algorithm is being investigated.

Speed-up is a good indicator of the performance of a parallel algorithm because it interprets how the computational speed changes in response to variation in number of processing units, $N$. Speed-up, $S$ is defined as $S = \frac{T_{ref}}{T_N}$. Here, $T_{ref}$ is defined as overall time required to solve a problem of interest using reference number of processing units (PU), $N_{ref}$. Similarly, $T_N$ is defined as overall time required to solve *the same* problem using $N$ PUs. In an ideal case, there is a linear variation. Usual approach is to set $T_{ref}$ as the overall time required for sequential computation (reference number of PUs is one in such a case [Gourdain et al, 2009a]). However, the algorithm is inherently written for parallel applications; hence, in this study, the reference number of PUs are set to the number of cores in a node supplied by the computational facilities.

Platforms used for conducting scalability tests are Colosse server of CalculQuebec in Canada [Url-1, 2017] which has 960 x Intel Xenon X5560 CPUs with 2.8 GHz speed and Sariyer server of National High Performance Computing Center of Turkey [Url-2, 2017] which has 48 x Intel Xenon E5-2680 v4 CPU with 2.4GHz speed. Each node has 8 cores in Colosse and 28 cores in Sariyer. Hence, $N_{ref}$ is taken as 8 for Colosse server and 28 for Sariyer server.

A test case of a channel flow is prepared with 10 million elements to test the scalability of the solver. The task is to perform 1000 iterations with different core numbers in the given platforms, up to 512 cores in Colosse server and 392 cores in Sariyer server.

Figure 1 shows the variation of speed up with respect to number of processing units $N_{PU}$. Red line represents the ideal case where the speed of executing the code is doubled when doubling the number of PUs. Speed-up results at Sariyer server is excellent, scalability performance being close to ideal case where the worst speed-up is the last test made with 392 cores which was able to provide 93% of the ideal speed up. Also the least speed-up performance is seen at the test with highest number of PUs in Colosse server with 77% of the ideal speed-up.

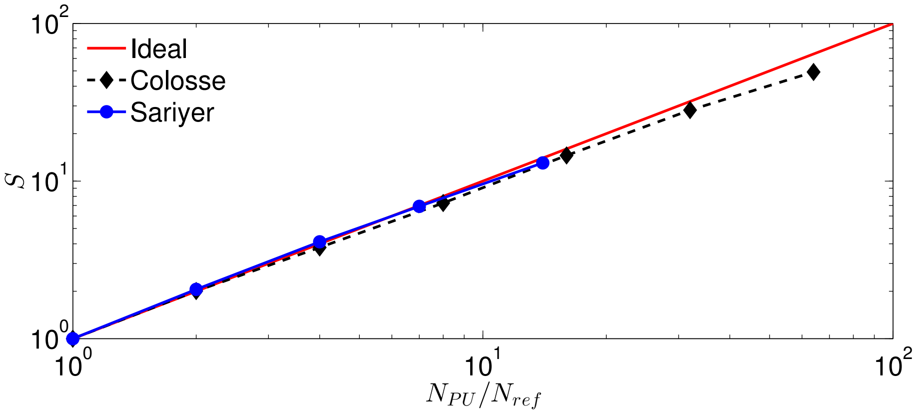


Figure 1: Speed-up, $S$ versus number of processing units, $N$.

## LID DRIVEN CAVITY FLOW

Lid-driven cavity flow is a well documented problem of interest to many researchers seeking a broader knowledge on the physics of fluid flows. One of the main reasons for this interest is the formation of various structures in a plain geometry. Depending on the Reynolds number, $Re = U_0 h/\nu$, where $U_0$ is the velocity of the moving lid, $h$ is the edge length of the cavity and $\nu$ is the kinematic viscosity of the fluid, multiple counter-rotating vortices, Taylor-Görtler type vortices, flow bifurcations, and transition to turbulence can be observed in addition to the persistent primary vortex at the center [Shankar and Deshpande, 2000; Prasad and Koseff, 1989]. Flow in the cavity is driven by the shear force originated from the moving wall at the top surface. In addition to the stationary primary vortex at the center of the domain, smaller turbulent structures at different scales can also be observed near the corners and edges of the cavity. These secondary vortices, rotating in the opposite direction of the primary vortex, increase the complexity of the momentum transfer in the flow. The characteristics of the flow is well documented by both numerical and experimental studies [Bouffanais et al, 2007; Prasad and Koseff, 1989; Leriche and Gavrilakis, 2000]. It also has been a common benchmark test to validate the solvers developed.

In this study, LES of lid-driven cavity flow at $Re = 12000$ is presented. At this Reynolds number, flow near the downstream eddy becomes fully turbulent since the Reynolds number increases beyond the critical value, which is $10000$ [Bouffanais et al, 2007]. Computational domain is a cubical cavity whose width, length and depth are $h$. Flow is induced by imposing a uniform tangential velocity, $U_0$, in the streamwise direction at the top surface (lid). All other boundaries are treated as no-slip walls. Simulations are performed using grids with 0.125M, 1M and 2M hexahedral elements and these simulations are going to be referred as LES1, LES2 and LES3, respectively. Statistics are accumulated after an initial transition has passed and this transition period is taken to be full development of the primary vortex. Time averaged velocities and root-mean-square (rms) fluctuations are non-dimensionalized by using the reference velocity, $U_0$ and Reynolds stress term is non-dimensionalized by using $U_0^2$. Also data collected from a probe that is placed at the location; $x/h = 0.8937$, $y/h = 0.0306$ and $z/h = 0.66855$ is used. Results obtained are compared with DNS data for $Re = 12000$ where $129^3$ Chebyshev polynomials were used in the grid [Leriche and Gavrilakis, 2000] and experimental data for $Re = 10000$ [Prasad and Koseff, 1989].

### Effects of Artificial Dissipation Constants

Although the artificial dissipation is integrated to the code for better numerical characteristics and eliminating the problems arising from central difference scheme, JST scheme is observed to be over dissipative for LES simulations [von Kaenel, R., 2003] which leads to decreased turbulent activity. In order to minimize the dampening effect, trials are made for lowering the constants $k^{(2)}$ and $k^{(4)}$ in dissipation scheme. LES2 grid is used for these studies. Results from two cases where $k^{(2)}$ and $k^{(4)}$ constants are taken as $6/25$ and $1/256$ respectively in LES2-high dissipation case and $6/250$ and $1/2560$ in LES2 case are presented.

Figure 2(a) shows the energy density spectrum at the probe location given in the previous section for these two simulations. It can be seen that small structures(high frequency) are effected significantly by the dissipation scheme and energy contained in these high frequency motions gets lower with high dissipation constants. Also the range of flow structures formed during simulation is reduced as fre-

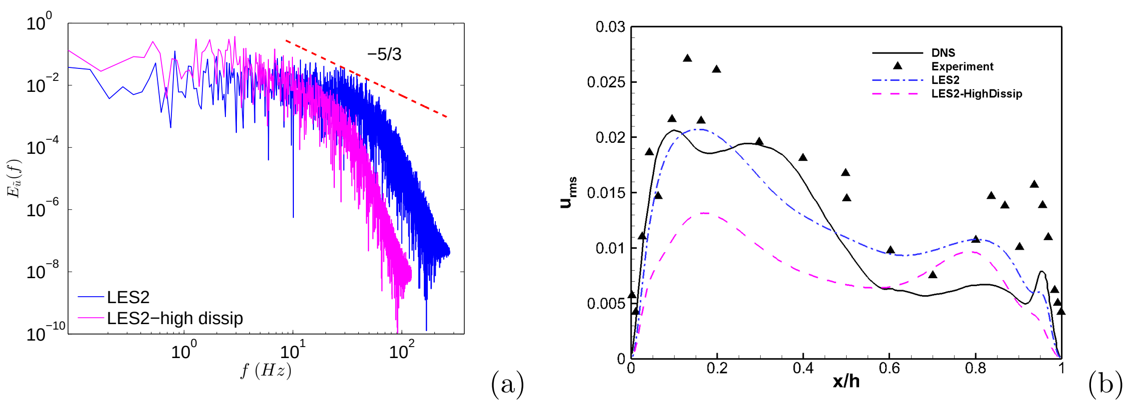


Figure 2: Effects of JST dissipation constants, on energy density spectrum (a) and $u_{rms}$, plotted on $x/h = 0.5$ at the plane $z/h = 0.5$ (b).

quencies higher than 100 $Hz$ cannot be appropriately represented in the energy density spectrum. Changes in turbulent statistics can also be seen in figure 2(b), as the $u_{rms}$ (root-mean square of streamwise velocity fluctuation) values are examined at the midplane. With high dissipation parameters, fluctuating component of velocity decreases significantly compared to low dissipation case. By considering these results, it is evident that the dissipation scheme influences the scales resolved by the solver and prevents the formation of smaller scales. Lower dissipation constants are used in further analyses for better capturing the turbulent structures.

### Effects of Grid Resolution

As referred above, simulations are made by using three different grids with varying resolutions, results obtained by using these grids are compared in this section. Sub-grid scale model is used for representing small structures that are not being fully resolved by the solver. Hence changing the resolution of the grid leads to involvement of the sgs model in different extents. Figure 3 shows the sgs eddy viscosity values obtained from instantaneous data on $z/h = 0.5$ plane. With the direct comparison of eddy viscosity values, it can be noticed that the LES1 is not as successful as LES3 when capturing the small structures formed in the regions where high gradients are observed due to the strong influence of the lid, but rather relies mainly on the sub-grid model to simulate the outcomes of these smaller scales.

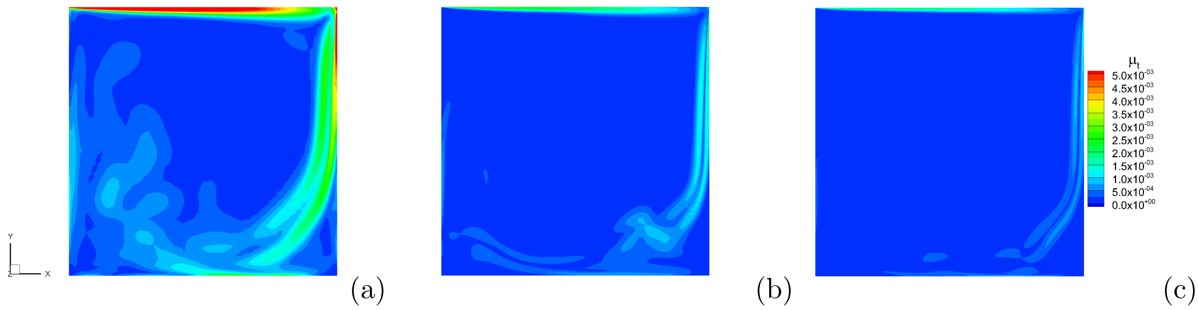


Figure 3: Instantaneous sgs eddy viscosity contours at the midplane $z/h = 0.5$, LES1 (a), LES2 (b) and LES3 (c).

Figure 4(a) shows the energy density spectrum acquired from LES1, LES2 and LES3. The energy levels of high frequency motions escalate as the grid resolution is increased. The increment in turbulent activity can also be observed from figure 4(b), where $v_{rms}$ results are given for three cases on $x/h = 0.5$ at the midplane. As grid is successively refined, more and more fine scale turbulent structures are resolved and computations eventually turn into DNS.

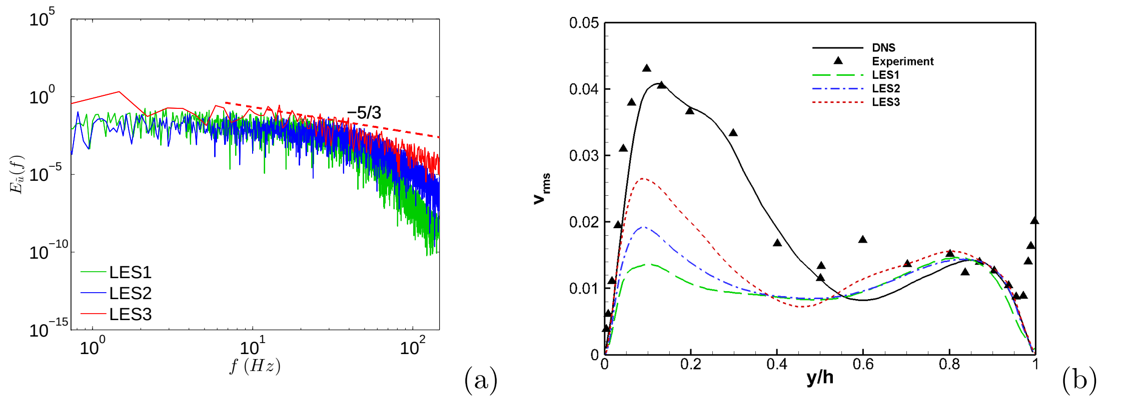


Figure 4: Energy density spectrum (a) and $v_{rms}$ results on $x/h = 0.5$ at the plane $z/h = 0.5$ (b).

Figure 5 shows the one-dimensional profiles of the average velocity field and its fluctuations from LES3. DNS and experimental data is used for direct comparison. It can be seen that main features of the flow are successfully captured. Mean velocities on the vertical and horizontal centerlines at the midplane $z/h = 0.5$ are well-matched with the compared results. Comparison of rms fluctuations and Reynolds shear stress $\overline{uv}$ are made in figure 5(c) and (d), where a significant similarity to reference data is obtained with slight deviations near the wall.

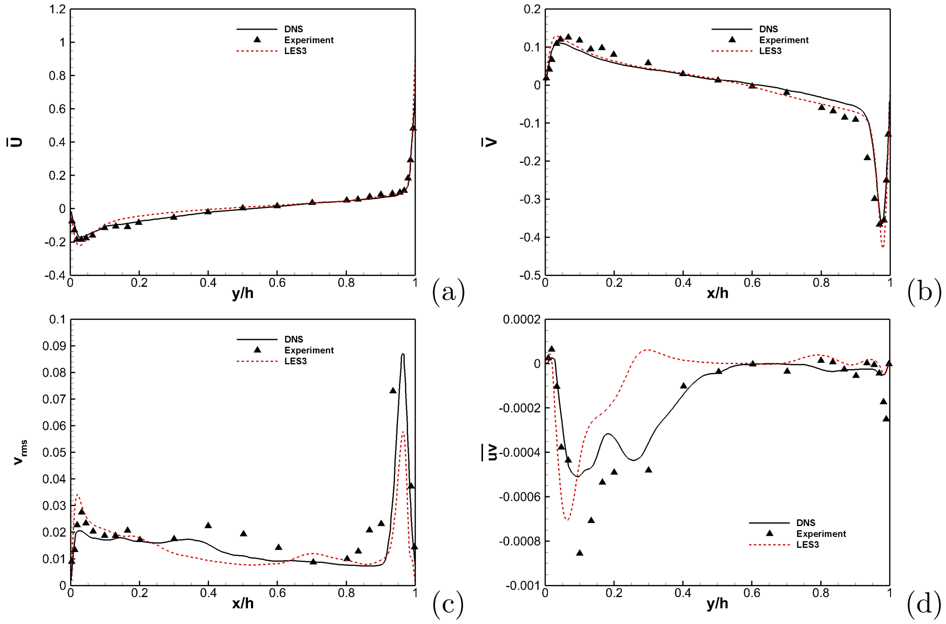


Figure 5: $\overline{U}$ on the $x/h = 0.5$ line (a), $\overline{V}$ on the $y/h = 0.5$ line (b), $v_{rms}$ values on $y/h = 0.5$ (c), $\overline{uv}$ on $x/h = 0.5$ line (d) at the midplane $z/h = 0.5$; DNS data [Leriche and Gavrilakis, 2000], experimental data [Prasad and Koseff, 1989].

## FLOW OVER T106 TURBINE BLADE

As stated in previous sections, *lestr3d* solver is developed for simulating wall-bounded turbulent flows mainly in aerospace applications. Thus, flow over T106 turbine blade is an important case for assessing the capabilities of the solver for similar flows. Details of the flow has been investigated in detail both experimentally [Langston et al, 1977; Duden et al, 1999; Stieger and Hoodson , 2004] and numerically [Wissink and Rodi , 2006; Sandberg et al , 2012; Sarkar , 2009] in past studies.

In this section, results from two different cases with and without endwall is presented. These cases are named LPTe and LPT, rspectively. A grid with approximately 3.2M elements is used for LPT. But in LPTe, where the complex flow structures originated from endwall effects are investigated, a grid with 4.4M elements is used with an increasing element density near endwall. With the definition of the x as the streamwise axis and z as the spanwise axis, boundary conditions used in these simulations can be better explained. In LPT case, periodic boundary condition is used in z direction to represent the infinitely long blade. But for the LPTe case, the flow is confined in spanwise direction with walls. No-slip boundary condition is used at the bottom (-z plane) and slip wall is used at the top (+z plane) of the domain. Periodic boundary condition is used in both cases in boundaries facing y direction which represents the linear cascade. Also the uniform inlet is used for both simulations with flow coming with an angle of 45° with respect to inlet surface normal. The simulations are performed at $Re = 80000$, where $Re$ is defined as, $Re = U_0 c/\nu$. Here, $U_0$ being the velocity at the inlet plane, $c$ is the chord length and $\nu$ is the kinematic viscosity of the fluid.

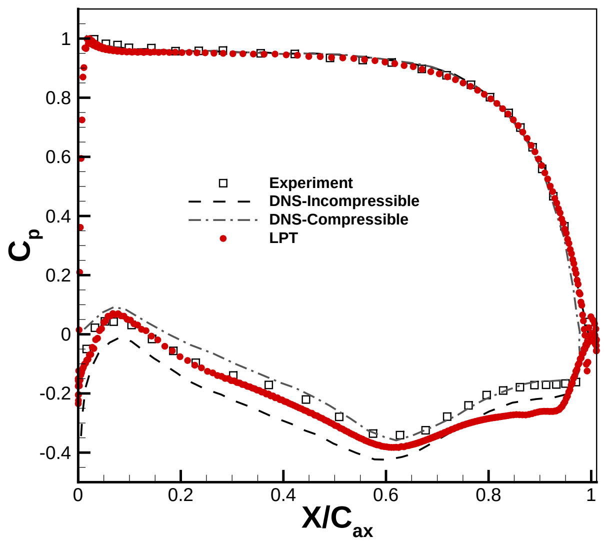


Figure 6: Mean pressure coefficient on the surface of the blade in LES of LPT (without endwall), Experiment [Wissink and Rodi , 2006], DNS-Incompressible [Wissink and Rodi , 2006], DNS-Compressible [Sandberg et al , 2012].

Distribution of the mean pressure coefficient, $C_p$ along the blade axial chord, $C_{ax}$ is shown in figure 6 compared with experiment [Wissink and Rodi , 2006] and DNS [Wissink and Rodi , 2006; Sandberg et al , 2012] data. $C_p$ distribution is in good agreement with references apart from a slight difference at the separated zone on the suction side of the blade.

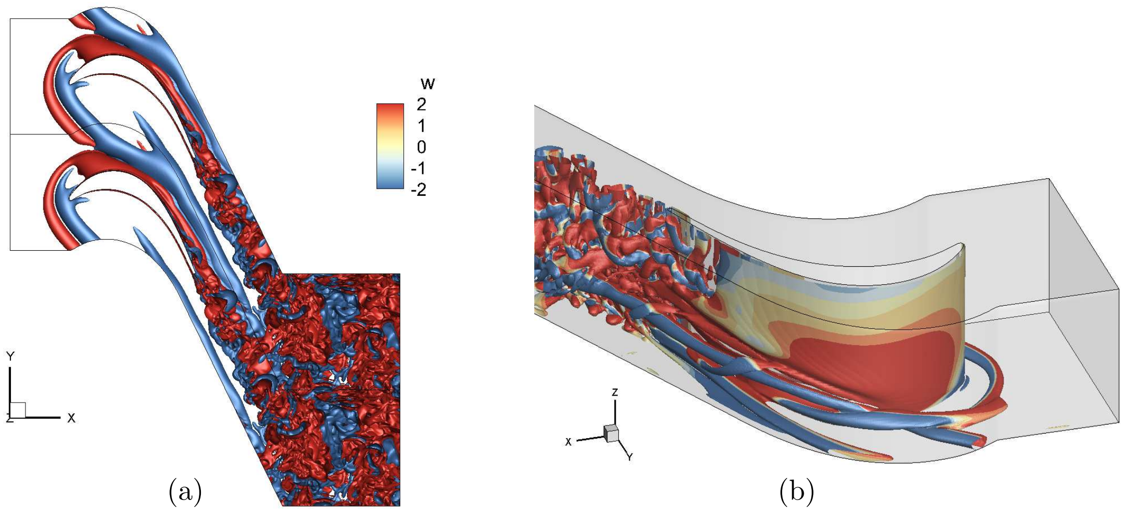


Figure 7: $w$ isosurfaces (a) and second invariant of velocity gradient tensor isosurfaces (b) colored by using $w$ magnitudes in LPTe(with endwall)

Isosurfaces in figure 7 are drawn using the spanwise velocity w and the second invariant of velocity gradient tensor [Hunt et al , 1988] calculated from the instantaneous flow field data. Structures formed due to endwall effects can be seen from the figure. With the use of periodic boundary condition in y direction, interaction between the blades can also be observed. Apart from that, turbulence formed with the separation can be seen near the trailing edge. Capturing these turbulent structures enables us to gain information about the complex relations between the flow and the blade performance.

## CONCLUSION

Details about the developed, large eddy simulation algorithm, *lestr3d* are presented. Numerical method is explained and scalability performance of the algorithm is shown with results from different platforms. The capability of the solver to simulate wall bounded turbulent flows is assessed with lid driven cavity flow. The effects of artificial dissipation and grid resolution are discussed with the help of the acquired data. Further results from the simulation of T106 turbine blade are given which has a significance for not only showing the performance of the algorithm to handle complex flow structures, but also for presenting the implementation of the code to contemporary engineering problems.

## ACKNOWLEDGEMENTS

This work is funded by the Scientific and Technological Research Council of Turkey (TUBITAK) under grant number 114M593. Simulations presented in this study are performed by using the computational sources supplied by Center of High Performance Computing of Turkey (UHeM).

# References

Andersson, N., Eriksson, L.-E. and Davidson, L. (2015) *Large-eddy simulation of subsonic jets and their radiated sound* AIAA Journal, Vol 43, No 9, p: 1-14.

Bouffanais, R., Deville, M. O., Leriche, E. (2007) *Large-eddy simulation of the flow in a lid-driven cubical cavity*, Physics of Fluids, Vol 19, p: 120.

Duden, A., Raab, I., Fottner, L.(1999) *Controlling the secondary flow in a turbine cascade by three-dimensional airfoil design and endwall contouring*, , J. Turbomach.. 121(2) 191-199.

Erlebacher, G, Hussaini, M. Y., Speziale, C. G. and Zang, T. A. (1992) *Towar the large-eddy simulation of compressible turbulent flows* J. Fluid Mech., Vol 238, p: 155-185.

Falese, M, Gicquel, L. Y. M. and Poinsot, T. (2009) *LES of bifurcation and hysteresis in confined annular swirling flows*, Computers and Fluids, Vol 89, p: 167-178.

Frink, N. T. (1994) *Recent progress toward a three-dimensional Navier-Stokes solver* AIAA Paper in 32nd Aerospace Sciences Meeting, Nevada, US, Jan 1994.

Gourdain, N., Gicquel, L., Montagnac, M., Vermorel, O., Gazaix, M., Staffelbach, G., Garcia, M., Boussuge, J.-F. and Poinsot, T. (2009) *High performance parallel computing of flows in complex geometries: I. Methods* Computational Science & Discovery, Vol 2.

Gourdain, N., Gicquel, L., Staffelbach, G., Vermorel, O., Duchaine, F., Boussuge, J.-F., and Poinsot, T. (2009) *High performance parallel computing of flows in complex geometries: II. Applications*, Computational Science & Discovery, Vol 2.

Hunt, J. C. R. and Wray, A. A. and Moin, P. (1988) *Edddies, stream, and convergence zones in turbulent flows*, , Center for Turbulence Research Report 193-208.

Karypis G. and Kumar V. (1999) *A fast and high quality multilevel scheme for partitioning irregular graphs*, SIAM J. Scientific Comput., Vol 20, No 1, p: 359-392.

Lacaze, G. and Oefelein, J. C. (2015) Development of quality assessment techniques for large eddy simulation of propulsion and power systems in complex geometries, **Technical Report**, Sandia National Laboratories.

Langston, L.S., Nice, M.L., Hooper R.M. (1977) *Three dimensional flow within a turbine cascade passage*, J. Eng. and Power. 99(1) 21-28.

Leriche, E. and Gavrilakis, S. (2000) *Direct numerical simulation of the flow in the lid-driven cubical cavity*, Phys. Fluids Vol 12, No 6, p: 1363-1376.

Prasad, A. and Koseff, J. (1989) *Reynolds number and end-wall effects on a lid-driven cavity flow*, Physics of Fluids, Vol 1, No 2, p: 208218.

Sandberg, R. D., Pichler, R., Chen, L., (2012) *Assessing the sensitivity of turbine cascade flow to inflow disturbances using direct numerical simulation*, , 13th International Symposium for Unsteady Aerodynamics, Aeroacoustics and Aeroelasticity in Turbomachinery(ISUAAAT), Tokyo, Japan 2012.

Sarkar, S. (2009) *Influence of wake structure on unsteady flow in a low pressure turbine blade passage*, , J. Turbomach. 131(4).

Shankar, P. N. and Deshpande, M. D. (2000) *Fluid mechanics in the driven cavity*, Annu. Rev. Fluid Mech., Vol 32, p:93-136.

Smagorinsky, J. (1963) *General circulation experiments with the primitive equations I. The basic experiment*, Monthly Weather Review, Vol 91, No 3, p: 99-164.

Stieger, R.D., Hoodson, H.P. (2004) *The transition mechanism of highly loaded low-pressure turbine blades*, , J. Turbomach.. 126(4) 536-543.

Url-1 *www.calculquebec.ca*, last retrieved in 16 July 2017.

Url-2 *http://www.uhem.itu.edu.tr/index.php/donanim-2/*, last retrieved in 16 July 2017.

Url-3 *http://www.cerfacs.fr/cfd/*, last retrieved in 17 July 2017.

Url-4 *http://su2.stanford.edu/*, last retrieved in 17 July 2017.

Url-5 *http://www.openfoam.com/*, last retrieved in 17 July 2017.

von Kaenel, R. (2003) *Large-eddy simulation of compressible flows using the finite-volume method*, Ph. D. thesis, Swiss Federal Institute of Technology Zürich.

Wissink, J. G., Rodi, W., (2004) *Direct numerical simulations of transitional flow in turbomachinery*, , J. Turbomach.. 110 668-678.